Magnesium Hydroxide Dehydroxylation: In Situ Nanoscale Observations of Lamellar Nucleation and Growth

Michael J. McKelvy,*[,†,‡] Renu Sharma,[†,‡] Andrew V. G. Chizmeshya,[†] R. W. Carpenter,[†,‡] and Ken Streib[†,‡]

Center for Solid State Science and Science & Engineering of Materials PhD Program, Arizona State University, Tempe, Arizona 85287-1704

Received August 22, 2000. Revised Manuscript Received December 4, 2000

Lamellar dehydroxylation mechanisms are important in understanding highly reactive nanocrystal oxide formation as well as a variety of applied lamellar hydroxide reaction processes. These mechanisms have been observed for the first time via in situ nanoscale imaging for the prototype lamellar hydroxide: $Mg(OH)_2$. Environmental-cell, dynamic high-resolution transmission electron microscopy was combined with advanced computational modeling in discovering that lamellar nucleation and growth processes govern dehydroxylation. The host lamella can guide the formation of a solid solution series of lamellar oxyhydroxide intermediates en route to oxide formation. This investigation opens the door to a deeper, atomic-level understanding of lamellar dehydroxylation reaction processes, nanocrystal oxide formation, and the range of potential new intermediate materials and third component reaction pathways they can provide.

Introduction

Lamellar dehydroxylation/rehydroxylation processes are an integral component of modern technology. Applications range from highly reactive oxide nanoparticle formation, for example, MgO nanocrystals,[1−9] to worldwide $Ca(OH)_2$/CaO use for flue gas desulfurization,[10,11] to the exploration of Mg-rich lamellar hydroxide minerals as candidate materials for CO_2 mineral sequestration.[12−17] Because of its chemical and structural simplicity, $Mg(OH)_2$ is an important model system to probe lamellar hydroxide dehydroxylation mechanisms at the atomic level, their role in nanocrystal oxide formation, and their potential to enhance industrially important third-component reactions.

Mineral and synthetic $Mg(OH)_2$ dehydroxylation to MgO (periclase) has been widely studied because of its fundamental interest and importance in industrial MgO production.[1,2] The process has been generally viewed as a two-phase ($Mg(OH)_2$ and MgO) process, which maintains the crystallographic orientational relationship shown in Figure 1.[1,3−9] The resulting MgO properties and its broad range of industrial uses depend strongly on the dehydroxylation conditions, which provide pathways to materials ranging from high-density, low surface-area refractories (calcined above 1800 °C) to low-density, high surface-area (10−200 m^2/g) materials with high chemical reactivity (calcined between 500 and 900 °C).[1,2] As expected, the high chemical reactivity of the latter materials is associated with their high surface area,

* To whom correspondence should be addressed. E-mail: mckelvy@asu.edu.
† Center for Solid State Science.
‡ Science & Engineering of Materials PhD Program.

(1) Green, J. *J. Mater. Sci.* **1983**, *18*, 637.
(2) Maniocha, M. L. *Min. Eng.* **1997**, *2*, 26.
(3) Gordon, R. S.; Kingery, W. D. *J. Am. Ceram. Soc.* **1966**, *49*, 654.
(4) Moodie, A. F.; Warble, C. E. *J. Cryst. Growth* **1986**, *74*, 89.
(5) Kim, M. G.; Dahmen, U.; Searcy, A. W. *J. Am. Ceram. Soc.* **1987**, *70*, 146.
(6) Naono, H. *Colloids Surf.* **1989**, *37*, 55.
(7) Thangaraj, N.; Westmacott, K. H.; Dahmen, U. *Ultramicroscopy* **1991**, *37*, 362.
(8) MacKenzie, K. J. D.; Meinhold, R. H. *Thermochim. Acta* **1993**, *230*, 339.
(9) Kim, M. G.; Dahmen, U.; Searcy, A. W. *J. Am. Ceram. Soc.* **1988**, *71*, C373.
(10) Lachapelle, D. G. U.S. Environmental Protection Agency Doc. EPA/600/F-95/013, Aug, 1995.
(11) *International Energy Agency Coal Research—The Clean Coal Centre* web site (http://www.iea-coal.org.uk/iea1.htm).

(12) Exponentially increasing atmospheric CO_2 levels and their potential adverse environmental consequences (e.g., global warming) have spurred substantial interest in the capture and sequestration of stationary source CO_2 emissions, that is, CO_2 sequestration.[13] Unlike other potential CO_2 sequestration technologies that offer long-term storage (e.g., ocean and geological sequestration), mineral sequestration provides permanent CO_2 disposal through the formation of geologically stable mineral carbonates, such as magnesite, $MgCO_3$.[14−17] Mg-rich layered hydroxide minerals, such as brucite and the serpentines, offer a class of materials that can potentially address this issue by providing permanent, low-cost CO_2 sequestration via carbonation reaction engineering. Enhancing their carbonation reaction rates is key to lowering process cost, as longer reaction times dramatically increase cost.[15−17] This is the primary focus of the CO_2 Mineral Sequestration Working Group managed by the U.S. Department of Energy, consisting of members from the Albany Research Center, Arizona State University, Los Alamos National Laboratory, the National Energy Technology Laboratory, and Science Applications International Corporation. The potential of serpentine carbonation as a viable CO_2 mineral sequestration technology has been recognized in the formation of the Zero Emission Coal Alliance, an alliance of researchers from Los Alamos National Laboratory and U. S. and Canadian coal suppliers and utilities.

(13) Halmann, M.; Steinberg, M. *Greenhouse Gas Carbon Dioxide Mitigation, Science and Technology*; Lewis Publishers: London, 1999.
(14) Seifritz, W. *Nature* **1990**, *345*, 486.
(15) Lackner, K. S.; Wendt, C. H.; Butt, D. P.; Joyce, E. L., Jr.; Sharp, D. H. *Energy* **1995**, *20*, 1153.
(16) Butt, D. P.; Lackner, K. S.; Wendt, C. H.; Conzone, S. D.; Kung, H.; Lu, Y. C.; Bremser, J. K. *J. Am. Ceram. Soc.* **1996**, *79*, 1892.
(17) Lackner, K. S.; Butt, D. P.; Wendt, C. H. *Energy Convers. Mgmt.* **1997**, *38*, S259.

10.1021/cm000676t CCC: $20.00
Published on Web 02/07/2001

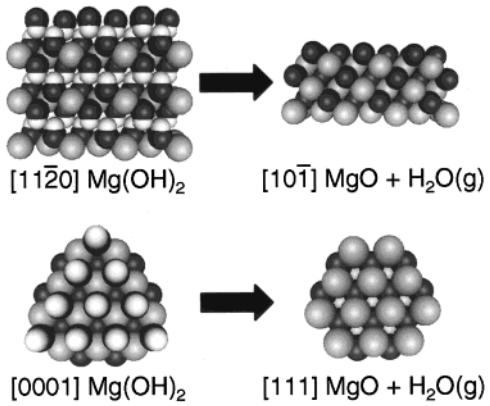

Figure 1. Lamellar magnesium hydroxide structure viewed parallel (upper left) and perpendicular (lower left) to the host layers and the equivalent orientations observed for MgO after dehydroxylation. As the MgO layers restack during dehydroxylation, there is an ~50% decrease in the interlamellar distances. There is also an ~5% decrease in the intralamellar Mg−Mg packing distance from 3.15 Å for $Mg(OH)_2$ to 2.98 Å for MgO. Light gray, dark gray, and white spheres represent Mg, O, and H atom positions, respectively. Note: the crystallographic relationships shown above emphasize the relationship between the initial and final structures, not their morphology.

which can lead to heats of formation as high as 17 kcal/mol above that observed for bulk MgO.[18]

Low-temperature $Mg(OH)_2$ calcination leads to the formation of nanostructured MgO materials, with morphological similarities to the host $Mg(OH)_2$ crystal.[3−7,9] These materials are typically comprised of intergrown cubic MgO nanocrystals, with edge dimensions ranging from about 1 to several nanometers, depending on the dehydroxylation conditions. Larger than normal interatomic distances have been occasionally observed for MgO during its initial formation, which has been ascribed to a coherency strain between MgO and $Mg(OH)_2$[3] or MgO surface-adsorbed water,[5] which is retained up to 550 °C. The high surface areas and heats of formation observed for the final-state nanostructured MgO materials are directly associated with the high chemical reactivity observed for "light-burned" or "caustic-calcined" forms of magnesia.[1,2]

Although $Mg(OH)_2$ dehydroxylation has been extensively studied, the atomic-level nature of the process is poorly understood, especially in its early stages. The process has been widely studied by transmission electron microscopy. However, the sensitivity of $Mg(OH)_2$ to electron beam heating has limited these studies to low magnification, where dehydroxylation rates could be reasonably controlled.[3−5] To circumvent these limitations, we used environmental-cell (E-cell) dynamic high-resolution transmission electron microscopy (DHRTEM) to directly observe the atomic-level nature of the dehydroxylation process for the first time. Incorporation of water vapor inhibits dehydroxylation, allowing direct imaging of the hydroxide lamella during dehydroxylation. These observations are combined with in situ electron diffraction investigations and ab initio density functional theory (DFT) and nonempirical electron-gas modeling studies to better elucidate the atomic-level process and the intermediate materials formed.

(18) Beruto, D.; Rossi, P. F.; Searcy, A. W. *J. Phys. Chem.* **1985**, *89*, 1695.

Experimental Section

Natural single-crystal brucite ($Mg(OH)_2$) from Delora, Canada, was used as the starting material. Elemental analysis by proton-induced X-ray emission, Rutherford backscattering, and total carbon analysis showed the material to contain 0.16% Mn, 0.06% C, 0.01% Cl, and 0.01% Si impurities by weight. X-ray powder diffraction was used to structurally characterize the starting material [$a = 3.147(1)$ Å and $c = 4.765(1)$ Å], which is in good agreement with the known parameters for brucite [$a = 3.147$ Å and $c = 4.769$ Å].[19] E-cell DHRTEM samples were prepared in a He glovebox by either cold crushing at −196 °C or scraping the crystal with a razor blade. Crystals were then dry loaded on to holey-carbon-coated copper grids for DHRTEM analysis. Samples prepared in this fashion contain some thin crystal fragments with their lamella oriented nearly perpendicular to the grid, which facilitates imaging parallel to the lamella. Freshly formed single-crystal fragments were selected for study to minimize the effects of surface impurities (e.g., surface carbonation) on the observed atomic-level dehydroxylation mechanisms.

In situ studies of $Mg(OH)_2$ dehydroxylation were performed using a Philips 430 HRTEM (300 kV; 2.3 Å point to point resolution) equipped with a Gatan imaging filter (GIF) and a 0−5 Torr E-cell. Dehydroxylation was induced by electron beam heating and resistive heating using the sample holder, both with and without the presence of water vapor. Direct imaging of the reaction was recorded on videotape in real time (30 frames/s). Water vapor (e.g., ~1 Torr) was required to slow the dehydroxylation process sufficiently for direct imaging. A Digital Micrograph (Gatan, Inc.) was used to analyze the interlamellar spacings in four-frame time-averaged images of the dehydroxylation process parallel to the brucite layers. Selected area diffraction (SAD) patterns of the reaction process were recorded as a function of time using internal gold island diffraction standards and photographic plates.

Ab initio density functional theory calculations and nonempirical electron-gas modeling based on the VIB method[20] were used to investigate the relative stability, elastic behavior, and structural trends of intermediate lamellar oxyhydroxide materials as a function of composition. The objective is to probe the intermediate lamellar oxyhydroxide materials that can form prior to final-state nanostructured oxide formation. These studies are carried out to provide insight into the role such intermediates can play in (i) the lamellar dehydroxylation processes directly observed by DHRTEM, (ii) the formation of the final nanostructured MgO product, and (iii) third-component reactions involving dehydroxylation.

These studies follow earlier work on simple hydroxides based on the closely related PIB method.[21] The compositional behavior was investigated using periodic lamellar phases to represent discrete compositions in the oxyhydroxide solid solution series. Using a brucite-like motif (with space group symmetry $P\bar{3}m1$), bulk periodic ordered phases of stoichiometry $Mg_{x+y}O_x(OH)_{2y}$ were structurally optimized and then used to compute the enthalpies, free energies of formation, and bulk moduli. The formation energy (per mole of Mg) of these intermediates is defined as the energy difference between the ordered oxyhydroxide and the sum of the energies of equivalent stoichiometric amounts of MgO and $Mg(OH)_2$. The free energy at each composition was simply estimated by adding the entropy of ideal mixing to the computed internal crystal energies.

Ab initio density functional theory calculations based on the GGA method[22,23] were also carried out for bulk MgO, $Mg(OH)_2$, and $Mg_{x+y}O_x(OH)_{2y}$ and molecular H_2O. These calculations yield structural parameters typically within a percent of the corresponding experimental values. Our GGA estimate of the

(19) U. S. Nat. Bur. Stand. Circ. **1956**, *539*, 6, 30.
(20) Chizmeshya, A.; Zimmermann, F. M.; LaViolette, R. A.; Wolf, G. H. *Phys. Rev. B* **1994**, *50*, 15559.
(21) LeSar, R.; Gordon, R. G. *Phys. Rev. B* **1982**, *25*, 7221.
(22) We employ the PWGGA functional as implemented within the CRYSTAL98 periodic DFT and Hartree−Fock program. Saunders, V. A. et al. *CRYSTAL98 User's Manual*; University of Torino, 1998.

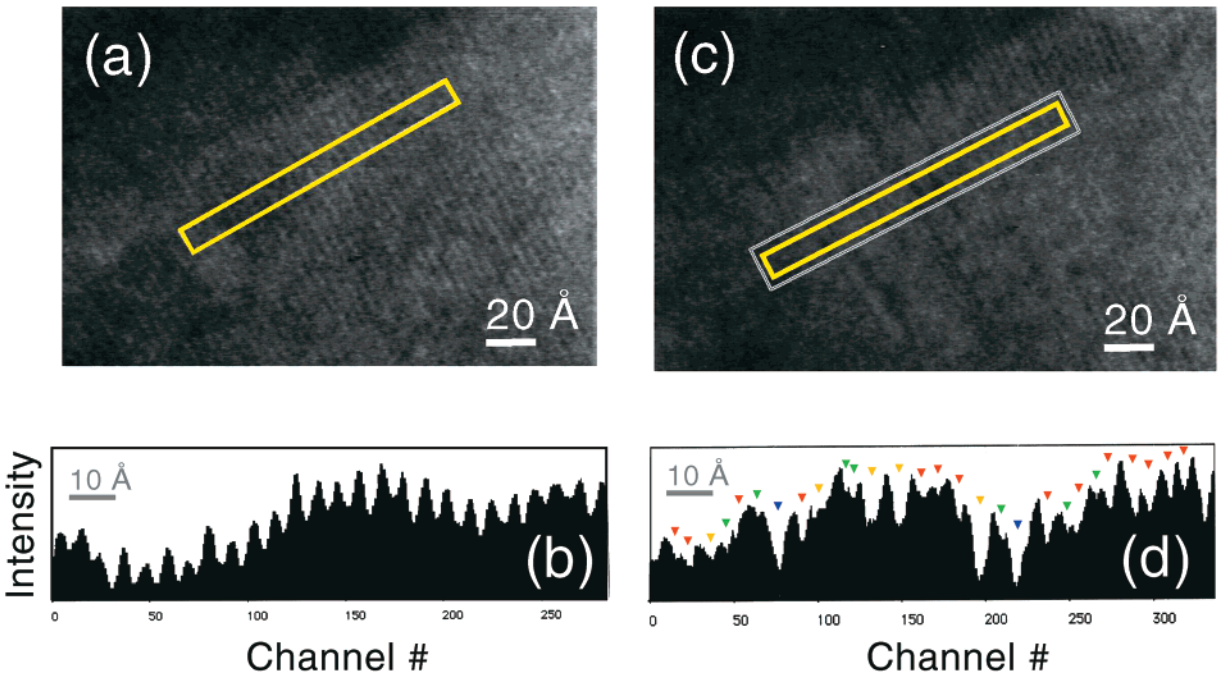

Figure 2. In situ DHRTEM observations (~1 Torr H_2O) parallel to the $Mg(OH)_2$ lamella prior to and during dehydroxylation taken from four-frame averaged videotape sequences. (a) Bright-field image of the host $Mg(OH)_2$ lamella prior to dehydroxylation. (b) An intensity line profile perpendicular to the host layers calculated by a Digital Micrograph for the region shown in (a). All interlamellar peak-to-peak spacings measure 4.8 ± 0.5 Å. (c) A bright-field image of the host $Mg(OH)_2$ lamella during dehydroxylation. Line profiles from interlamellar regions, such as those shown in (c), show discrete oxide, hydroxide, and oxyhydroxide (adjacent single oxide and hydroxide layers) interlamellar spacings. (d) An intensity line profile from the interior region shown in (c). The observed spacings fall into three groups: (i) 2.5 ± 0.4 Å (7 spacings marked in green; MgO spacing 2.43 Å via XPD), (ii) 4.9 ± 0.5 Å (14 spacings marked in red; $Mg(OH)_2$ spacing 4.77 Å via XPD), and (iii) 7.3 ± 0.5 Å (5 spacings marked in yellow; MgO + $Mg(OH)_2$ spacing 7.20 Å). Two additional spacings of 9.0 Å are also observed (marked in blue), which may correspond to $Mg_3O_2(OH)_2$ oxyhydroxide lamella (9.6 Å) or to lamellar regions that are currently dehydroxylating within the region shown in (c).

enthalpy of formation for $Mg(OH)_2$ from MgO and H_2O (g), 17.9 kcal/mol,[24,25] compares very well with the observed value of 19.4 kcal/mol,[26] while a relative energy for the 50% dehydroxylation intermediate $^1/_2\{E[Mg_2O(OH)_2] - E[MgO] - E[Mg(OH)_2]\}$ of 2.8 kcal/mol is obtained. This is to be compared with the VIB estimate of 2.6 kcal/mol. The ab initio calculations were also used to derive a hydroxyl binding potential, required in the ionic VIB (or PIB) models to stabilize the (OH) bond. In previous work[21] this bond was explicitly constrained, thereby precluding a quantitative treatment of dynamical and elastic behavior.

Results and Discussion

The lamellar nature of the dehydroxylation process can be seen in E-cell DHRTEM observations parallel to the $Mg(OH)_2$ layers shown in Figure 2. Prior to dehydroxylation, the $Mg(OH)_2$ lamella are observed to have regular interlayer repeats of 4.8 ± 0.5 Å, in good agreement with those measured by X-ray powder diffraction (4.765 Å). Direct observations during dehydroxylation reveal a low-dimensional process guided by the parent $Mg(OH)_2$ lamella. Analysis of time-averaged videotape sequences shows the formation of intermediate lamellar oxyhydroxide regions during dehydroxylation. These regions contain discrete oxide, hydroxide, and oxyhydroxide lamella, with the oxyhydroxide lamella comprised of adjacent oxide and hydroxide layers. Oxide lamella generally nucleate and grow at the expense of the parent hydroxide lamella until dehydroxylation is complete. The random distribution of the oxide, oxyhydroxide, and hydroxide layers observed suggests the intermediate oxyhydroxide regions locally exhibit lamellar solid-solution-like behavior between the oxide and hydroxide layers.

Substantial intralamellar strain is expected to accompany the formation of oxyhydroxide regions due to the 5% hexagonal packing mismatch between adjacent oxide and hydroxide lamella (e.g., the in-plane Mg−Mg distance in ideal (111) MgO lamella is 2.98 Å, whereas 3.15 Å is observed for $Mg(OH)_2$). Diffraction of the in situ dehydroxylation process perpendicular to the $Mg(OH)_2$ lamella was used to follow the structural behavior of both the oxyhydroxide and hydroxide regions throughout dehydroxylation, as shown in Figure 3. Two distinct materials are observed during dehydroxylation: (i) the parent hydroxide and (ii) the oxyhydroxide, which nucleates and grows, eventually yielding the oxide, at the expense of the hydroxide. The lamellar structure of the parent $Mg(OH)_2$ appears to remain unchanged throughout the process, as it is slowly consumed by oxyhydroxide/oxide formation and growth. On the other hand, the oxyhydroxide regions that nucleate and grow

(23) We carried out a full suite of GGA calculations of the compression equation of state of MgO, $Mg(OH)_2$, and several oxyhydroxide intermediates. Equilibrium lattice constants and internal structural parameters reproduced experimental values to within 1%. The calculated bulk moduli of MgO and $Mg(OH)_2$ are 158 and 49 GPa, respectively (ab initio GGA), 162 and 61 GPa (VIB), compared with the experimental values of 160 GPa (MgO) and 46 GPa ($Mg(OH)_2$).

(24) We follow Refson, K. et al.[25] in adding the sublimation energy of ice to our molecular H_2O energy to obtain the formation energy at 0 K.

(25) Refson, K.; Wogelius, R. A.; Fraser, D. G.; Payne, M. C.; Lee, M. H.; Milman, V. *Phys. Rev. B* **1995**, *52*, 10823.

(26) James, A. M.; Lord, M. P. *Macmillan's Chemical & Physical Data*; Macmillan Press LTD: London, 1992.

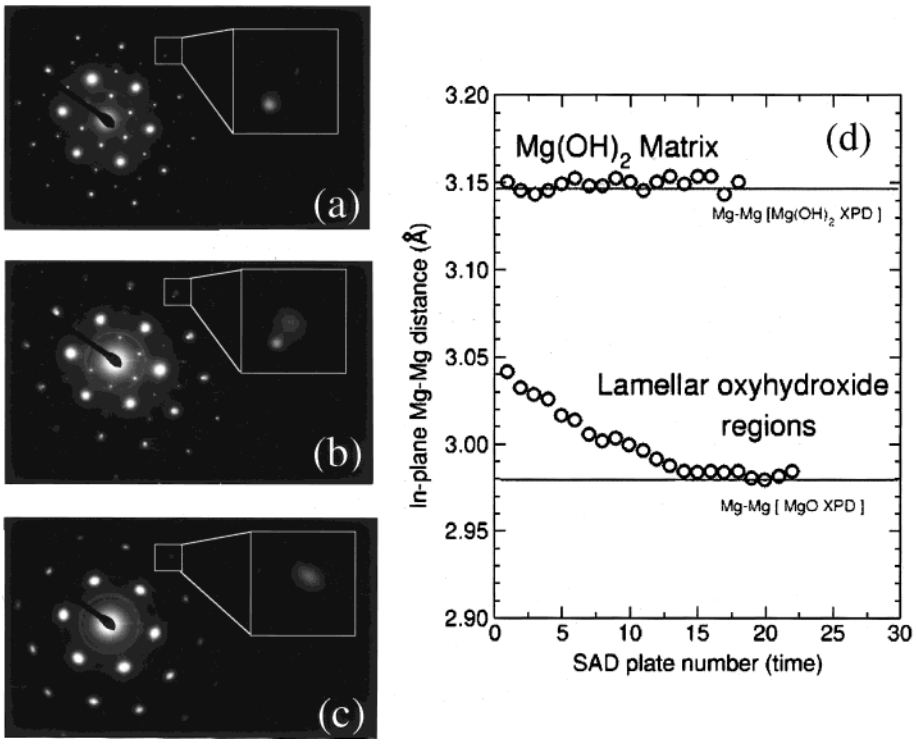

Figure 3. Selected area diffraction (SAD) study of the in situ dehydroxylation process perpendicular to the brucite layers: (a) SAD of $Mg(OH)_2$ prior to dehydroxylation. (b) SAD of the $Mg(OH)_2$ matrix containing lamellar oxyhydroxide regions during dehydroxylation. (c) SAD of the product MgO aligned along ⟨111⟩. (d) Intralamellar Mg−Mg distances observed by SAD during dehydroxylation. The hydroxide SAD pattern slowly fades during dehydroxylation, until only the oxyhydroxide/oxide pattern remains. The Mg−Mg packing distances based on X-ray powder diffraction for $Mg(OH)_2$ and MgO are shown for comparison.

in the parent hydroxide matrix are initially observed with an intermediate intralamellar packing distance of 3.04 Å, which is more than half the intralamellar contraction expected for dehydroxylation. The substantial contraction of the intralamellar packing in oxyhydroxide nuclei suggests that they initially formed with relatively high concentrations of oxide lamella. As dehydroxylation proceeds, the in-plane packing distance slowly decreases to that observed for MgO as more hydroxide layers are converted to oxide lamella. This suggests that the oxyhydroxide regions exhibit novel two-dimensional solid-solution-like behavior, where the intralamellar packing distance is a function of the average number of hydroxide and oxide layers present locally. Such behavior is reminiscent of Vegard's law for two-component metal solid solutions,[27] which predicts that the cell dimensions of the solid solution vary linearly with the concentration of the solute component.

Ab initio DFT calculations and nonempirical electron-gas modeling studies provide insight into the relative stability, elastic behavior, and structural trends of the intermediate oxyhydroxides, as shown in Figures 4 and 5. As discussed earlier, the compositional behavior is investigated using periodic lamellar phases to represent discrete compositions in the oxyhydroxide solid solution series. The energies shown are relative to two-phase [$Mg(OH)_2$ + MgO] mixtures. Overall, the model is representative of the intermediate materials formed until extensive dehydroxylation leads to final-state nanostructured MgO product formation, where surface energy contributes significantly to the formation energy.

(27) Wells, A. F. *Structural Inorganic Chemistry*, 5th ed.; Clarendon Press: Oxford, 1984; p 1293.

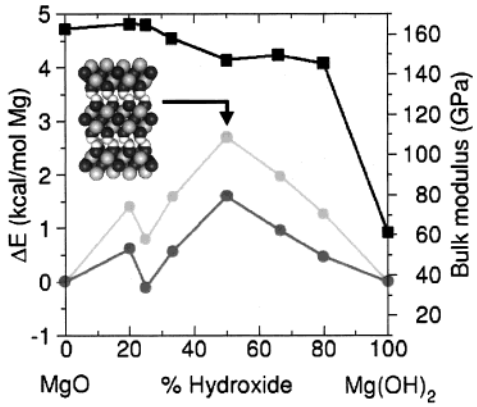

Figure 4. Free energies (dark gray) and enthalpies (light gray) for representative lamellar oxyhydroxide intermediate materials ($Mg_{x+y}O_x(OH)_{2y}$: x oxide layers for every $2y$ hydroxide layers) relative to stoichiometrically equivalent amounts of MgO and $Mg(OH)_2$. The bulk moduli of the intermediates are shown in black (boxes). The inset shows the structure of the $Mg_2O(OH)_2$ oxyhydroxide intermediate, which contains an equal number of oxide and double-hydroxide layers, viewed parallel to the layers. The light gray, dark gray, and white spheres represent the Mg, O, and H atom positions, respectively. The above results apply to the dehydroxylation process, which leads to MgO nanostructure formation. Hence, they do not include the surface energy associated with the formation of the final-state nanostructured MgO product.[18]

The formation energy dependence on nanostructure particle size will be examined in detail in a subsequent modeling study.

Both thermodynamic stability and elastic behavior appear key to the observed lamellar dehydroxylation process and the intermediate phases formed. Intermediate oxyhydroxides containing low or high concentrations

Table 1. In-Plane Packing Distances Observed by SAD for the Oxyhydroxide, $Mg_{x+y}O_x(OH)_{2y}$, Regions and the $Mg(OH)_2$ Matrix during In Situ Dehydroxylation[a]

study	$Mg(OH)_2$ matrix (packing distance)	$Mg_{x+y}O_x(OH)_{2y}$ (packing distance)	$Mg_{x+y}O_x(OH)_{2y}$ composition (% $Mg(OH)_2$)
Gordon and Kingery[3]	3.15 Å	3.14 → 2.98 Å	94% → 0%
Kim et al.[5]	3.15 Å	3.00 → 2.98 Å	12% → 0%
present study	3.15 Å	3.04 → 2.98 Å	35% → 0%

[a] The composition range is determined by comparison with Figure 5.

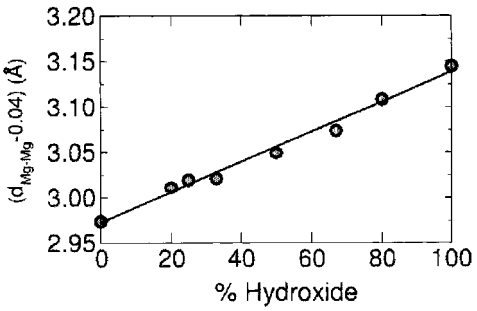

Figure 5. In-plane (e.g., Mg−Mg) packing distances for the intermediate lamellar oxyhydroxides shown in Figure 4, as a function of hydroxide layer composition. A small systematic overestimate of 0.04 Å in all the computed distances, determined by VIB-based nonempirical electron gas modeling, is inferred by comparison with the known values for MgO and $Mg(OH)_2$. The computed values shown are shifted to allow for the overestimate.

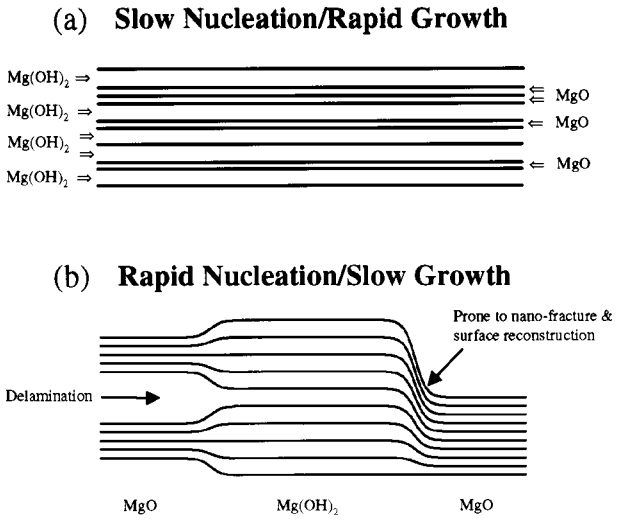

Figure 6. Models of lamellar nucleation and growth processes during $Mg(OH)_2$ dehydroxylation. A model for relatively slow nucleation and rapid growth leading to oxyhydroxide intermediate formation is shown in (a). The process proceeds in a largely homogeneous fashion locally, consistent with previous low-magnification TEM and diffraction observations of $Mg(OH)_2$ dehydroxylation.[3] A model for relatively rapid nucleation and slow growth leading to primarily two-phase, $Mg(OH)_2$ + MgO, dehydroxylation behavior is shown in (b). This process proceeds in a locally heterogeneous fashion, consistent with a separate low-magnification TEM and diffraction investigation.[5] The high cumulative strain associated with edge dislocation formation and motion can facilitate nanoscale cracking and fragmentation, leading to commonly observed crystal fracture and the formation of final-state nanostructured MgO product materials.[3−7,9] The intermediate energy of the oxyhydroxides can combine with the local elastic deformation (e.g., bending) energies of the layers to guide the dehydroxylation process.

of oxide lamella are more stable, but not dramatically so, as all compositions become thermodynamically accessible (as well as kinetically accessible) within the temperature range 400−800 °C. The oxyhydroxide bulk moduli reveal a dramatic increase in material stiffness early during dehydroxylation, substantially increasing the host-layer bending (deformation) energy needed for dehydroxylation. This significantly slows dehydroxylation for all but low oxide layer concentrations. The greater lamellar flexibility present during initial dehydroxylation combines with the lower stability of intermediate composition oxyhydroxides to promote relatively rapid dehydroxylation to higher oxide layer concentrations. This explains the high concentration of oxide lamella initially found in the oxyhydroxide regions observed by electron diffraction and the enhanced resistance of these regions to further dehydroxylation.

The presence of lamellar oxyhydroxide solid solution behavior during dehydroxylation is confirmed by the in-plane structural behavior of the $Mg_{x+y}O_x(OH)_{2y}$ oxyhydroxide solid solution series found via VIB-based nonempirical electron gas modeling. Figure 5 shows that two-dimensional Vegard's-law-like behavior is predicted for the oxyhydroxides,[27] as observed in the above SAD studies. As a result, determination of the in-plane packing distance during dehydroxylation provides insight into the composition of the corresponding lamellar oxyhydroxide regions in situ. Table 1 shows the range of oxyhydroxide compositions observed based on the present investigation and re-evaluation of previous in situ SAD observations of the dehydroxylation process.[3,5] In each study, the in-plane packing distance and composition of the host $Mg(OH)_2$ matrix remains unchanged during dehydroxylation and is largely unaffected by oxyhydroxide nucleation and growth. However, essentially the full range of packing distances and compositions has been observed during nucleation and growth of the lamellar oxyhydroxide solid solution series, indicating these new lamellar materials are broadly accessible, at least locally.

Overall, dehydroxylation proceeds by lamellar nucleation and growth. Initially, an oxide layer begins to form by dehydration of a double-hydroxide $Mg(OH)_2$ layer:

$$\cdots OH/Mg/OH/OH/Mg/OH\cdots \rightarrow \cdots OH/Mg/O/Mg/OH\cdots + H_2O \quad (1)$$

Growth occurs via the formation of additional partial/full oxide layers nearby, creating lamellar oxyhydroxide regions, which can grow parallel and perpendicular to the lamella in the $Mg(OH)_2$ matrix. More generally, this process can exhibit primarily lamellar oxyhydroxide intergrowth or two-phase (oxide + hydroxide) behavior via relatively slow nucleation/fast growth or fast nucleation/slow growth, respectively, as shown in Figure 6. Differences observed in previous low-magnification TEM imaging and diffraction dehydroxylation studies are consistent with competition between such relatively slow-nucleation/fast-growth[3] (significant oxyhydroxide

intermediate formation) and fast-nucleation/slow-growth[5] (primarily two-phase, $Mg(OH)_2$ + MgO) processes. Higher and lower reaction rates (e.g., temperatures) are generally expected to favor nucleation and growth, respectively.

The large volume decrease during dehydroxylation (~50%), together with the formation of morphological relics of the parent $Mg(OH)_2$ particles, has long been associated with MgO nanostructure formation. At the atomic level, nanostructure formation can directly result from the lamellar nucleation and growth process, with competition between rapid nucleation/slow growth and slow nucleation/rapid growth governing the nanostructures formed. Host-layer bending during lamellar nucleation and growth induces substantial local elastic strain, as shown in Figure 6. The resulting strain can induce cracking and delamination at the nanometer level, as observed during lamellar deintercalation processes.[28] Such cracking and delamination is further promoted by the rapid increase in stiffness of the host lamella early during dehydroxylation (Figure 4), which favors layer cracking over layer bending. The resulting nanofragmentation can then provide the high surface mobility required for the well-known formation of nanostructured MgO pseudomorphs.[3−7,9] Competition between slow-nucleation/fast-growth and fast-nucleation/slow-growth processes will have a pronounced effect on elastic strain locally, suggesting the intriguing possibility of controlling reactive nanostructure formation by guiding the nucleation and growth characteristics of the dehydroxylation process.

Discovery of the lamellar nucleation and growth process also opens the door to a range of new $Mg_{x+y}O_x(OH)_{2y}$ materials, which are of interest in themselves and as intermediates for new reaction pathways. As new materials, they may offer the potential to combine and control some of the appealing properties associated with light-burned magnesia and small particle-size $Mg(OH)_2$.[1,2] As reaction intermediates, they can also provide new paths to enhance the rate of third-component reactions, such as the carbonation of Mg-rich lamellar-hydroxide minerals to lower CO_2 mineral sequestration process costs.[12] Recently, we have discovered a dramatic increase in gas-phase carbonation reactivity associated with simultaneous $Mg(OH)_2$ dehydroxylation/rehydroxylation processes, indicating transient intermediate (e.g., oxyhydroxide) formation can substantially enhance carbonation reactivity.[29] These studies are part of a larger joint research effort aimed at making zero-emission coal-fired power a reality.

Acknowledgment. We gratefully acknowledge the National Energy Technology Laboratory of the U.S. Department of Energy for support through Grants DE-FG26-98FT40112 and DE-FG26-99FT40580. The E-cell DHRTEM was conducted at the Center for High Resolution Electron Microscopy at Arizona State University. We also thank the Center for Solid State Science for use of the Goldwater Materials Science Laboratories, including the Materials Facility, the Goldwater Materials Visualization Facility, and the Ion Beam Analysis Facility.

CM000676T

(28) Sidorov, M. V.; McKelvy, M. J.; Sharma, R.; Glaunsinger, W. *J. Solid State Chem.* **1998**, *141*, 330.

(29) McKelvy, M. J.; Carpenter, R. W.; Sharma, R.; Bearat, H.; Streib, K. *Abstract and Research Accomplishments of University Coal Research Projects*; National Energy Technology Laboratory: Pittsburgh, 2000; p 108.